

RARE B MESON DECAYS

T.E. Browder*

Physics Department

University of Hawaii, Honolulu, HI 96822

ABSTRACT

This paper is based on a pedagogical lecture given at the SLAC Summer Institute on Particle Physics. I discuss basic experimental techniques for the study of rare B meson decays, review some old and new results from Belle, BaBar and CLEO and indicate possible future directions.

*Supported by the US Department of Energy

1 Introduction, Motivation and History

Rare decays even when they are not observed may provide essential clues to fundamental physics. A well-known example is the upper limit on the decay $K_L \rightarrow \mu^+ \mu^-$ and its influence on the construction of the Standard Model of particle physics.

Recall that in a physical picture with only three quarks u, d and s governed by Cabibbo mixing, there are large $s \rightarrow d$ transitions. These transitions occur because the d weak interaction eigenstate is an admixture of strong interaction eigenstates,

$$d_c = d \cos \theta_c + s \sin \theta_c \quad (1)$$

where d, s are the strong interaction eigenstates and θ_c is the Cabibbo angle. As a result, the weak neutral current, J_{NC}^0 ,

$$J_{NC}^0 = u\bar{u} + d_c\bar{d}_c + s_c\bar{s}_c \quad (2)$$

$$= u\bar{u} + d\bar{d} \cos^2 \theta_c + s\bar{s} \sin^2 \theta_c + (s\bar{d} + \bar{s}d) \cos \theta_c \sin \theta_c \quad (3)$$

The term $(s\bar{d} + \bar{s}d) \cos \theta_c \sin \theta_c$ is a measure of the size of direct *flavor changing neutral current* $s \rightarrow d$ transitions and is not particularly suppressed. Yet $s \rightarrow d$ transitions were not observed.¹

In 1970, Glashow, Iliopoulos and Maiani (GIM)² introduced the c (charm) quark to cancel these troublesome and unobserved transitions. There are two doublets (u, d_C) , (c, s_C) with

$$d_C = d \cos \theta_c + s \sin \theta_c \quad (4)$$

$$s_C = -d \sin \theta_c + s \cos \theta_c \quad (5)$$

The weak neutral current has additional contributions

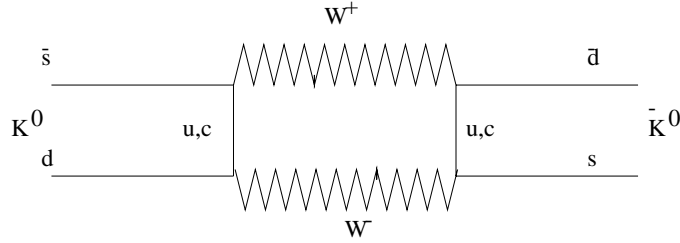
$$J_{NC}^0 = u\bar{u} + d_c\bar{d}_c + s_c\bar{s}_c + c\bar{c} \quad (6)$$

$$= u\bar{u} + c\bar{c} + (d\bar{d} + s\bar{s})(\cos^2 \theta_c + \sin^2 \theta_c) \quad (7)$$

$$+ (s\bar{d} + \bar{s}d - s\bar{d} - \bar{s}d) \cos \theta_c \sin \theta_c \quad (8)$$

$$= u\bar{u} + c\bar{c} + d\bar{d} + s\bar{s} \quad (9)$$

As a result of the introduction of the charm quark there is no longer the possibility of flavor changing neutral currents (FCNC) at first order. However, such FCNC can appear as higher order corrections. An example is $K^0 - \bar{K}^0$ mixing, which proceeds


 Fig. 1. Diagram for $K^0 - \bar{K}^0$ mixing

via a second order box diagram shown in Fig.1. The measured rate of transition of this *rare* decay allowed the quantitative prediction of m_C , the mass of the new charm quark.

Later, accelerators and experimenters were able to directly produce the charm quark. In 1974, teams at SLAC and Brookhaven led by Richter and Ting observed the J/ψ , a $c\bar{c}$ bound state.⁴

In the above example, measurements of rare decays at relatively low energies led the way to New Physics of higher energies. One might wonder whether if this is an anomalous historical example. However, there are other examples. For instance, the observation that large FCNC in B decays are absent from the first measurements at the CLEO experiment ruled out “top-less” models, with no t quark.⁵ The observation of large $B^0 - \bar{B}^0$ mixing at the ARGUS experiment in Hamburg^{6,7} suggested that m_t , the mass of the top quark, was much larger than the 30-40 GeV range suggested by UA1 and the existing theoretical prejudice of the time.⁸

Given these spectacular historical examples, we are motivated to study further rare decays of B mesons in order to learn about high mass scales that may not be directly accessible at current experiments.

2 Trees and Penguins/Experimental Techniques

What is a rare decay? A rare B decay is a decay that does not proceed by the dominant $b \rightarrow c$ transition. Examples of Feynman diagrams for such rare B decay are shown in Fig. 2. The decays either involve $b \rightarrow u$ transitions (Fig. 2(a),(c)), loop $b \rightarrow s$ transitions (Fig. 2(b)) or transitions with W-exchange or W-annihilation (Figs. 2(d),(e)). With the exception of the W-exchange and W-annihilation diagrams, the processes shown in Fig. 2 may have a anti-quark spectator \bar{d} or \bar{u} .

Let’s consider the example of $B^0 \rightarrow K^- \pi^+$ and $B^0 \rightarrow \pi^- \pi^+$ decays. Both are examples of “rare” decays although with the advent of the B factories there are now

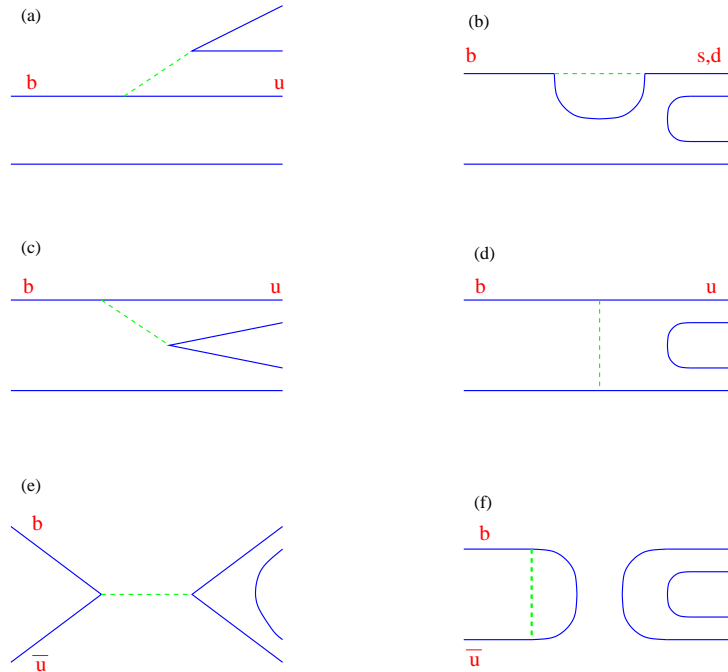


Fig. 2. Taxonomy of rare B decays. From left to right, top to bottom: (a) External spectator $b \rightarrow u$, (b) Penguin $b \rightarrow s$, (c) Internal spectator $b \rightarrow u$, (d) W-exchange (e) W-annihilation and (f) Hairpin diagram.

samples of these decays that contain hundreds of reconstructed events. Two amplitudes contribute to the decay $B^0 \rightarrow K^- \pi^+$. These are: a “penguin” $b \rightarrow s g^*$, $g^* \rightarrow u \bar{u}$ process and a “tree” $b \rightarrow u W^*$ transition followed by $W^* \rightarrow u \bar{s}$, where g^* means virtual gluon and W^* means virtual W. These same two contributions are present for $B \rightarrow \pi^+ \pi^-$ decays. However, in this case the tree $b \rightarrow u W^*$, $W^* \rightarrow u \bar{d}$ is not Cabibbo suppressed and the penguin process is $b \rightarrow d g^*$, $g^* \rightarrow u \bar{u}$ is suppressed compared to the $b \rightarrow s$ penguin that contributes to $B^0 \rightarrow K^- \pi^+$.

2.1 The origin of the term Penguin

One interesting historical sidelight is the origin of the term penguin. This was recently revealed to the general public in the Introduction to Misha Shifman’s 1999 book, *ITEP lectures on Particle Physics and Field Theory*.⁹ There, John Ellis of CERN, the inventor of the term recalls how the gluon interference diagram that was originally introduced by Shifman and coworkers came to be called a penguin diagram.

Here I quote: *One night in spring 1977, Ellis lost a bet during a game of darts. His*

penalty required that he use the word “penguin” in a journal article. “For some time, it was not clear to me how to get the word into this b quark paper that we were writing at the time”, Eliis wrote. “Then, one evening I stopped on my way back to my apartment to visit some friends living in Meyrin, where I smoked some illegal substance. *Later when I got back to my apartment and continued working on our paper, I had a sudden flash that the famous diagrams looked like penguins.* So we put the name into our paper, and the rest, as they say is history.”

2.2 Trees and Penguins

Let’s now return to the hierarchy of penguins and trees in B decay. For the two decays $B^0 \rightarrow K^- \pi^+$ and $B^0 \rightarrow \pi^0 \pi^+$, let’s examine the relative strengths of the two kinds of amplitudes, shown in Fig. 3, by counting the powers of the Wolfenstein parameter λ . In the $B^0 \rightarrow K^- \pi^+$ case, the penguin amplitude is $\mathcal{O}(\lambda^2)$ while the tree amplitude $\mathcal{O}(\lambda^4)$. This indicates the dominance of the penguin in $B^0 \rightarrow K^- \pi^+$ decay. In contrast, for the $B^0 \rightarrow \pi^+ \pi^-$ case, both the penguin and tree amplitudes are of the same order, $\mathcal{O}(\lambda^3)$.

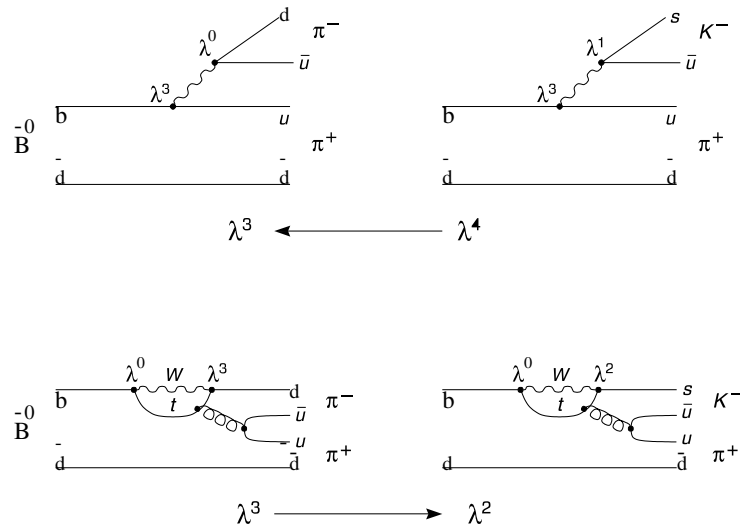


Fig. 3. Counting powers of the Wolfenstein parameter in rare decays.

The next important point to keep in mind is the interference of amplitudes. Even if one of the two amplitudes is smaller than the other, the interference term may be much larger than the square of the smaller amplitude and comparable in size to the modulus squared of the larger amplitude. The tree and penguin diagrams involve the CKM elements V_{bu} , V_{ts} and V_{td} , respectively. Therefore the tree and penguin diagrams

will usually have different weak phases and possibly different strong interaction phases. As a result, there is interference of tree and penguin diagrams, which leads to direct CP violation.

The direct CP violating asymmetry in B decay rates is

$$A_{dir} = \frac{\Gamma(\bar{B} \rightarrow \bar{f}) - \bar{\Gamma}(B \rightarrow f)}{\Gamma(\bar{B} \rightarrow \bar{f}) + \bar{\Gamma}(B \rightarrow f)} \quad (10)$$

$$A_{dir} = \frac{2r \sin \phi \sin \delta}{1 + r^2 + 2r \cos \phi \cos \delta} \quad (11)$$

where $r = |P|/|T|$ is the ratio of tree and penguin amplitudes, ϕ is the weak phase difference of the two amplitudes, and δ is the strong phase difference. From this equation, one can see that the direct CP asymmetry can be sizeable if the penguin (P) and (T) amplitudes are comparable in magnitude and if both strong (CP conserving) and weak phase differences (CP violating) are present.

We observed that the two amplitudes in $B^0 \rightarrow K^- \pi^+$ are $\mathcal{O}(\lambda^2)$ and $\mathcal{O}(\lambda^4)$ whereas those in $B \rightarrow \pi^+ \pi^+$ are both $\mathcal{O}(\lambda^3)$. Thus, by counting powers of λ , we might expect somewhat larger direct CP violating effects in $B \rightarrow \pi^+ \pi^-$ than in $B^0 \rightarrow K^- \pi^+$.

Another illustrative example is the decay mode $B^\pm \rightarrow K_S \pi^\pm$. In this case, there is a gluonic penguin contribution $b \rightarrow sg^*$, $g^* \rightarrow d\bar{d}$ but no $b \rightarrow u$ tree contribution. One can therefore use this mode to determine, $|P|$, the strength of the penguin amplitude. Moreover, since there is only one amplitude and no comparable interfering diagram, little or no CP violating asymmetry is expected in the Standard Model.¹² So measurements of CP asymmetry in this mode can be used to check for contributions beyond the Standard Model.

2.3 Experimental Techniques

We now discuss experimental techniques for the study of rare B decays. To be concrete we will focus on the simplest case, $B \rightarrow hh$ decay modes, where h may be either a neutral or charged pion or a kaon. Most of this discussion can easily be extended to other rare decay modes.

To isolate the signal, kinematic variables that take advantage of production at threshold and the small energy release in the decay $\Upsilon(4S) \rightarrow B\bar{B}$ are used. Reconstructed B meson decays are identified using the beam-constrained mass (or beam energy substituted mass) $M_{bc} \equiv \sqrt{E_{beam}^2 - p_B^2}$ and the energy difference $\Delta E \equiv E_B - E_{beam}$,

where E_{beam} is the half cms energy, and p_B and E_B are the reconstructed B candidate three-momentum and energy calculated in the center of mass system (cms).

The resolution in M_{bc} (M_{ES}) is ~ 2.7 MeV and is dominated by the accelerator beam energy spread rather than by the detector resolution and is almost one order of magnitude better than the resolution in invariant mass. This illustrates the power of kinematic reconstruction at threshold.

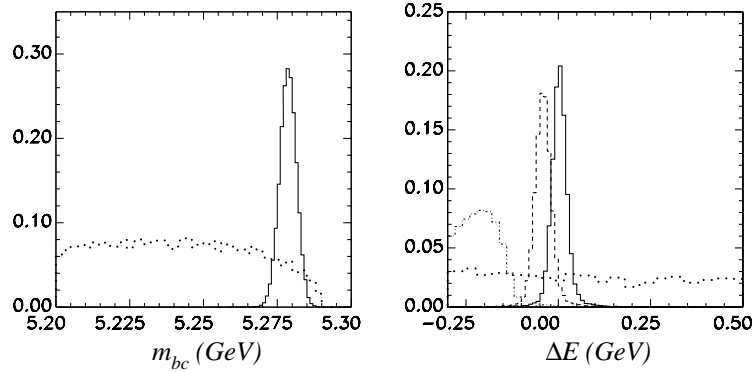


Fig. 4. Kinematic variables for a Monte Carlo simulation of the decay modes $B^0 \rightarrow K^- \pi^+$, $B \rightarrow \pi^+ \pi^-$ and their backgrounds.¹³ The dashed distribution is the continuum background while the hashed histogram is the contribution from three-body rare B decays.

In contrast, the resolution in ΔE is mode dependent and dominated by the detector resolution. Figs 4, 5 show a Monte Carlo simulation of the M_{bc} and ΔE distributions for two classes of rare decay modes: all charged final states and final states with one high momentum π^0 . The resolutions in M_{bc} for both classes of decays are the same, however, the ΔE resolutions are much broader for modes with π^0 s. As a result of energy leakage from the CsI(tl) crystals, there are also long asymmetric tails in these ΔE distributions. Fig. 4 also illustrates the difference between kaon and pion modes. For example, the modes $B^0 \rightarrow K^- \pi^+$ and $B^0 \rightarrow \pi^- \pi^+$ have identical M_{bc} distributions but are separated by about 45 MeV in ΔE .

2.3.1 Continuum suppression

Figure 6 shows the hadronic cross section as a function of e^+e^- center of mass energy. The $\Upsilon(4S)$, which is the lowest resonant state heavy enough to produce $B\bar{B}$ meson pairs, has a modest cross section $\mathcal{O}(1.05)$ nb and sits on a large background from non-

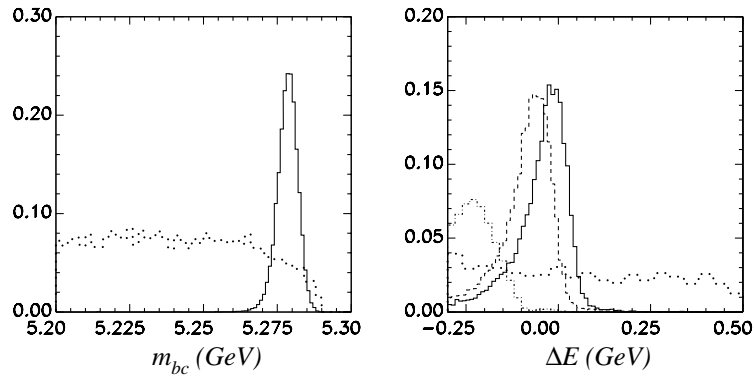


Fig. 5. Kinematic variables for a Monte Carlo simulation of the decay modes $B^+ \rightarrow K^+\pi^0$, $B^+ \rightarrow \pi^+\pi^0$ and their backgrounds.¹³ The dashed histogram is the continuum background while the hashed histogram is the contribution from three-body rare B decays.

resonant $e^+e^- \rightarrow q\bar{q}$ ($q = u, d, s, c$) processes. This non-resonant background is called “continuum” and is usually the dominant background for rare decay studies. As a result, much effort at the B factories has been devoted to continuum suppression techniques.

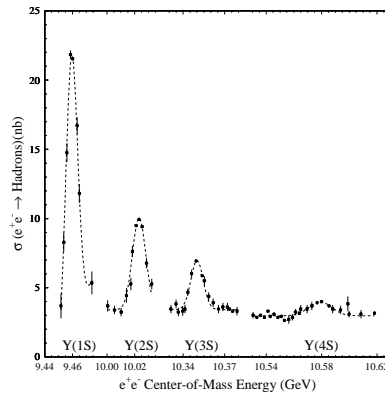


Fig. 6. The hadronic cross section in the 10 GeV energy region.

The underlying idea of continuum suppression techniques is the difference between the event shapes of continuum and $B\bar{B}$ events. Since continuum events are not resonant, there is a large energy release; the q and \bar{q} jets tend to emerge collimated and back to back. In contrast, due to the small energy release in the decay $\Upsilon(4S) \rightarrow B\bar{B}$, $B\bar{B}$ events tend to be spherical. A number of variables have been developed to quantify these differences.

The l -th Fox-Wolfram moment¹⁰ is defined by

$$H_l = \sum_{i,j} |p_i||p_j| P_l(\cos(\theta_{ij})) \quad (12)$$

where p_i is the i th particle's momentum, and $P_l(\cos \theta_{ij})$ is the l th Legendre polynomial. The argument of P_l is the cosine of the angle θ_{ij} between particles i and j .

The ratio of the second to zeroth Fox-Wolfram moments called R_2 , is a well-known inclusive variable for continuum suppression. Values of R_2 near 1 indicate a jetty, continuum-like event while values near 0 are characteristic of spherical $B\bar{B}$ -like events.

An extension of the Fox-Wolfram moments was introduced by R. Enomoto at Belle and is called the Super Fox-Wolfram. Here the terms in the summation in H_l are separated into three groups: terms involving particles i, j in the B candidate, terms with some particles in the B candidate and others from the rest of the event, and a third set involving only particles that do not belong to the B candidate. The modified Fox-Wolfram moments¹⁰ defined as

$$h_l^{so} = \sum_{i,j} p_i p_j P_l(\cos \theta_{ij}),$$

$$h_l^{oo} = \sum_{j,k} p_j p_k P_l(\cos \theta_{jk}),$$

where i enumerates B signal candidate particles (s particles) and j and k enumerate the remaining particles in the event (o particles).

The h_l^{so} terms contain information on the correlation between the B candidate direction and the direction of the rest of the event. The odd h_l^{oo} terms partially reconstruct the kinematics of the other B in the event while the even terms quantify the sphericity of the other side of the event. A six-variable Fisher discriminant (or linear combination) called the Super Fox-Wolfram (SFW) is defined as

$$SFW = \sum_{l=2,4} \alpha_l \left(\frac{h_l^{so}}{h_0^{so}} \right) + \sum_{l=1-4} \beta_l \left(\frac{h_l^{oo}}{h_0^{oo}} \right),$$

where α_l and β_l are the Fisher coefficients optimized for separation between continuum and $B\bar{B}$. Care is taken in the construction of the SFW not to include terms that are correlated with M_{bc} or ΔE .

The SFW variable is combined with the B flight direction with respect to the beam axis, $\cos \theta_B$, to form a single likelihood

$$\mathcal{L}_{B\bar{B}} = \mathcal{L}(SFW)_{B\bar{B}} \times \mathcal{L}(\cos \theta_B)_{B\bar{B}}$$

for signal and an equivalent product for continuum, $\mathcal{L}_{q\bar{q}}$. Continuum background is suppressed by cutting on the likelihood ratio

$$LR = \frac{\mathcal{L}_{B\bar{B}}}{\mathcal{L}_{B\bar{B}} + \mathcal{L}_{q\bar{q}}}.$$

These variables are shown in Fig. 7. As an example, Fig. 7 shows the $B^0 \rightarrow K^+\pi^-$ data sample before and after imposing the $LR > 0.8$ requirement.

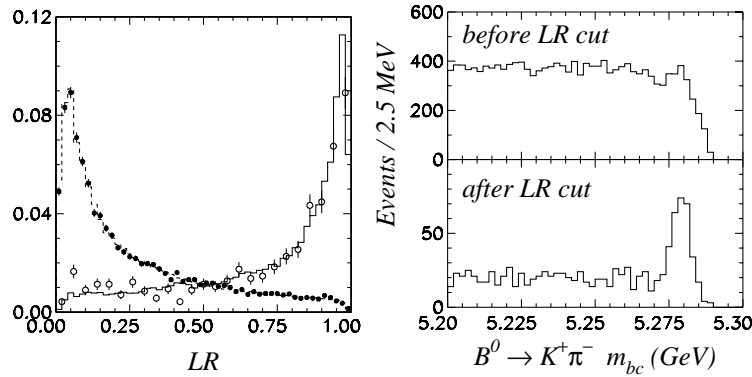


Fig. 7. The Belle event shape likelihood ratio and the effect of a cut on the signal to background ratio in $B^0 \rightarrow K^+\pi^-$.

Two quantities originally introduced by the CLEO experiment are also frequently used. The cosine of the angle between the thrust axis of the B candidate and the thrust axis of the remaining particles in the event is another powerful variable that can be used for continuum suppression. This variable is uniformly distributed for correctly reconstructed B candidates, but is strongly peaked near $\cos\theta = \pm 1$ for the jet-like continuum background.

The “virtual calorimeter” consists of the energies of tracks and showers in cones of increasing angle opposite the direction of the B candidate. Since continuum events are jettier than $B\bar{B}$ events, more energy is enclosed in the cones close to the recoil from the B candidate for continuum. Similarly, $B\bar{B}$ events contain more energy perpendicular to the B candidate axis. To maximize the continuum suppression power of the virtual calorimeter and thrust angle, a Fisher discriminant (or a linear combination with optimized weights) is calculated from the virtual calorimeter variables and the cosine of the thrust angle.

Other variations and combinations are possible. For example, BaBar requires $|\cos\theta_S| < 0.8$ and defines a Fisher discriminant $\mathcal{F} = 0.53 - 0.60 \times \sum_i p_i^* + 1.27 \times \sum_i p_i^* 2|\cos(\theta_i^*)|^2$,

where p_i^* is the momentum of particle i and θ_i is the angle between the thrust axis of the signal candidate and particle i . The * superscript indicates that the quantities are calculated in the CM frame.

2.3.2 Particle identification

The other challenging requirement for the detector is the separation of kaons from pions at high momentum. This is needed to distinguish $\bar{B}^0 \rightarrow \pi^+ \pi^-$ from $\bar{B}^0 \rightarrow K^- \pi^+$, which has similar kinematics and a branching fraction about three times larger. The original observations of most of the $B \rightarrow hh$ modes were reported by the CLEOII experiment, which had only dE/dx measurements from its central drift chamber to separate charged pions and kaons. At the B factory experiments two approaches to high momentum particle identification have been implemented. Both are based on the use of Cerenkov radiation.

At Belle, aerogel Cerenkov radiators are used. Blocks of aerogel are readout by fine-mesh phototubes that have high-gain and operate comfortably in a 1.5 Tesla magnetic field. Since the threshold for the aerogel is around 1.5 GeV, below this momentum K/π separation is carried out using high precision time-of-flight scintillators with resolution of 95 ps. The aerogel and TOF counter system are complemented by dE/dx measurements in the central drift chamber. The dE/dx system provides additional K/π separation around 2.5 GeV in the relativistic rise region as well as below 0.7 GeV. For high momentum kaons, an efficiency of 88% with a misidentification probability below 9% has been achieved.

At BaBar, Cerenkov light is produced in quartz bars and then transmitted by total internal reflection outside the detector through a water tank to a large array of phototubes where the Cerenkov ring is imaged. The detector is referred to by the acronym DIRC. It provides K/π separation that ranges from 8σ at 2 GeV to 2.5σ at 4 GeV.

The performance of the particle id systems can be calibrated with data. For example, continuum D^{*+} decays that have been kinematically identified with $D^{*+} \rightarrow D^0 \pi^+$, $D^0 \rightarrow K^- \pi^+$ can be used to measure efficiencies and fake rates in the high momentum range (1.5 – 4) GeV.

2.3.3 Fitting and signal extraction

To extract the signal yield BaBar, Belle and CLEO fit the ΔE distribution or M_{bc} distribution or perform a 2-dimensional fit to both ΔE and M_{bc} . Since modes with a

kaon substituted for a pion have identical distributions in M_{bc} but are separated in ΔE , ΔE is a crucial experimental distribution to judge the quality of a rare B decay signal.

The background in rare decays is dominantly continuum and can be modelled in M_{bc} by phase-space with a kinematic threshold. A good parameterization of this background is provided by the ARGUS function¹¹

$$\mathcal{A}(M_{bc}; M_0, \xi) = A_B M_{bc} \sqrt{1 - x_{bc}^2} e^{\xi (1 - x_{bc}^2)}, \quad (13)$$

where $x_{bc} = M_{bc}/M_0$ is the ratio of the beam constrained mass to its maximum value at the kinematic limit. The background ΔE distribution is typically linear for continuum, but is shifted in ΔE by at least $\sim \pm 140$ MeV for events when the final state differs from the signal by one pion.

Since the background in many rare decay modes is mostly continuum, events from a large “grand” sideband in $M_B, \Delta E$ outside the signal region can be used to provide a more accurate estimate of the background in the signal region, provided one knows the correct scaling factor from either data or Monte Carlo. Alternatively, events in the sideband can be used to model the *shape* but not normalization of the background in the signal region.

Additional statistical power may be obtained by performing a fit to not only ΔE and M_{bc} but shape variables and (particle identification) PID variables. In such cases, no cuts or minimal cuts are placed on the shape and PID variables. This has been done in some CLEO and BaBar analyses. However, $B\bar{B}$ backgrounds that peak in M_{bc} and correlations between the fit variables require special care.

2.4 Results on $B \rightarrow hh$ Decays

Since the M_{bc} distributions for $B^0 \rightarrow K^- \pi^+$ and $B \rightarrow \pi^+ \pi^-$ decays are identical, it is most instructive to examine the ΔE spectrum where there is some separation. The ΔE distributions from Belle and BaBar are shown in Figs. 8,9, respectively. In both sets of figures, there are small well separated reflections from misidentified $B \rightarrow \pi^+ \pi^-$ decays in the $B \rightarrow K^- \pi^+$ samples as well as contributions of misidentified $B \rightarrow K^- \pi^+$ decays in the $B \rightarrow \pi^+ \pi^-$ sample. The range in fig.8 is also large enough so that the contributions from three-body rare B decays is also visible.

The branching fractions measured by Belle,¹³ BaBar¹⁴ and CLEO¹⁵ are in good agreement and are given in Table 1. These results clearly show that $\mathcal{B}(B^0 \rightarrow K^- \pi^+) \gg \mathcal{B}(B \rightarrow \pi^- \pi^+)$ and that penguin diagrams are large. One consequence is that the

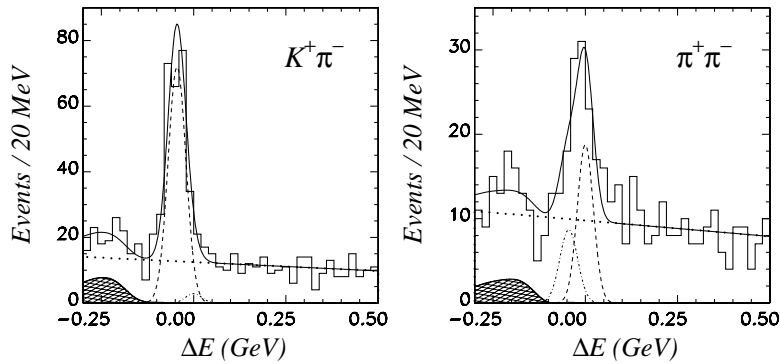


Fig. 8. The ΔE distributions from Belle's analysis of $B^0 \rightarrow K^-\pi^+$ and $B \rightarrow \pi^+\pi^-$ decays with 29 fb^{-1} . The $K\pi$ signal contains 218 ± 18 events while the $\pi\pi$ signal contains 67 ± 11 events.

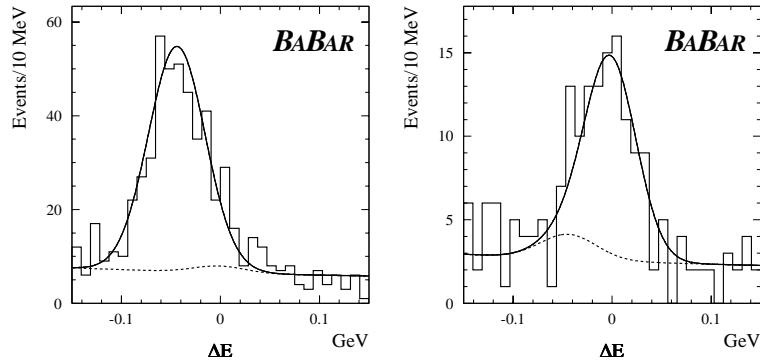


Fig. 9. The ΔE projections from BaBar's analysis of $B^0 \rightarrow K^-\pi^+$ and $B \rightarrow \pi^+\pi^-$ decays.

“penguin pollution” or contribution of penguin diagrams in time-dependent analyses of $B^0 \rightarrow \pi^+\pi^+$ cannot be neglected.

Searches for direct CP violation in the $B \rightarrow hh$ modes have been carried out by BaBar, Belle and CLEO. No clear indication has been observed. The results are given in Table 2. At the current level of precision, the asymmetry in detector response, which is at the $\mathcal{O}(1\%)$ level and can be checked with control samples, is not a major concern. Note that for CP eigenstate modes such as $B \rightarrow K^0\pi^0$ or $B \rightarrow \pi^+\pi^-$, flavor tagging of the accompanying B meson is required for the measurement.

As discussed in the lectures by MacFarlane, time-dependent CP asymmetries can be used to determine CKM angles, however it is also true that measurements of rates

Table 1. *Branching Fractions in units of 10^{-6} for $B \rightarrow K\pi$ and $B \rightarrow \pi\pi$ Modes. Note that the Belle results are based on analysis of 29 fb^{-1} and those of BaBar are from 81 fb^{-1} .*

	BaBar	Belle	CLEO
$B^0 \rightarrow \pi^+\pi^-$	$4.6 \pm 0.6 \pm 0.2$	$5.4 \pm 1.2 \pm 0.5$	$4.3^{+1.6}_{-1.4} \pm 0.5$
$B^+ \rightarrow \pi^+\pi^0$	$5.5^{+1.0}_{-0.9} \pm 0.6$	$7.4 \pm 2.2 \pm 0.9$	$5.6^{+2.6}_{-2.3} \pm 1.7$
$B^0 \rightarrow K^\pm\pi^\mp$	$17.9 \pm 0.9 \pm 0.7$	$22.5 \pm 1.9 \pm 1.8$	$17.2^{+2.5}_{-2.4} \pm 1.2$
$B^+ \rightarrow K^+\pi^0$	$12.8^{+1.2}_{-1.1} \pm 1.0$	$13.0^{+2.5}_{-2.4} \pm 1.3$	$11.6^{+3.0+1.4}_{-2.7-1.3}$
$B^+ \rightarrow K^0\pi^+$	$17.5^{+1.8}_{-1.7} \pm 1.3$	$19.4^{+3.1}_{-3.0} \pm 1.6$	$18.2^{+4.6}_{-4.0} \pm 1.6$
$B^0 \rightarrow K^0\pi^0$	$10.4 \pm 1.5 \pm 0.8$	$8.0^{+3.3}_{-3.1} \pm 1.6$	$14.6^{+5.9+2.4}_{-5.1-3.3}$

for rare B decay processes can give information about these unitarity triangle angles.

To understand this in a simple way and develop intuition, we follow the treatment of Fleischer and Mannel.¹⁶ We neglect the many possible complications and associated theoretical issues such as SU(3) breaking, rescattering (or final state interactions), electroweak penguins, and nono-factorizable. These are *important* and have been discussed in the SSI lectures by Ligeti¹⁷ and Kagan and in the theoretical literature.

First we write down the amplitudes for $B^+ \rightarrow K^0\pi^+$ (pure penguin) and $B^0 \rightarrow K^+\pi^-$ (penguin and $b \rightarrow u$ tree) in terms of the penguin P and T amplitudes and strong phases (δ_P, δ_T).¹⁶

$$A(B^+ \rightarrow K^0\pi^+) = P = -|P|e^{i\delta_P} \quad (14)$$

$$A(B^0 \rightarrow K^+\pi^-) = -[P + T] = -[-|P|e^{i\delta_P} + |T|e^{i\delta_T}e^{i\phi_3}] \quad (15)$$

Note that in the second amplitude, the CKM phase ϕ_3 (or γ) enters. We now rewrite

$$A(B^0 \rightarrow K^+\pi^-) = |P|e^{i\delta_P}[1 - re^{i\delta}e^{i\phi_3}] \quad (16)$$

where $r = |T|/|P|$ and $\delta = \delta_T - \delta_P$. To obtain rates, we square the amplitudes,

$$|A(B^+ \rightarrow K^0\pi^+)|^2 = |P|^2 \quad (17)$$

$$|A(B^0 \rightarrow K^+\pi^-)|^2 = |P|^2[1 - 2r \cos \delta \cos \phi_3 + r^2] \quad (18)$$

We then examine the ratio of the widths for $B^0 \rightarrow K^-\pi^+$ and $B^+ \rightarrow K^0\pi^+$,

$$R = \frac{\Gamma(B^0 \rightarrow \pi^\mp K^\pm)}{\Gamma(B^\pm \rightarrow \pi^\pm K^0)} = 1 - 2r \cos \delta \cos \phi_3 + r^2 \quad (19)$$

Table 2. 90% C.L. intervals or central values for CP Asymmetries in $B \rightarrow K\pi$ and $B \rightarrow \pi\pi$ Modes. The case of direct CP violation in $B \rightarrow \pi^+\pi^-$ is discussed later in the text.

	BaBar	Belle	CLEO
$B^+ \rightarrow \pi^+\pi^0$		$[-0.23, 0.86]$	
$B^0 \rightarrow K^\pm\pi^\mp$	$[-0.188, 0.016]$	$[-0.21, 0.09]$	$[-0.30, 0.22]$
$B^+ \rightarrow K^+\pi^0$	$[-0.24, 0.06]$	$[-0.35, 0.30]$	$[-0.67, 0.09]$
$B^+ \rightarrow K^0\pi^+$	$-0.17 \pm 0.10 \pm 0.02$	$[-0.10, 0.22]$	$[-0.22, 0.56]$
$B^0 \rightarrow K^0\pi^0$	$0.03 \pm 0.36 \pm 0.09$		

The ratio R is particularly attractive from both the experimental and theoretical point of view since systematics of both kind tend to cancel. Note that if the phase difference δ is small, then $R > 1$ (constructive interference) corresponds to $\phi_3 > 90^\circ$ and $R < 1$ (destructive interference) corresponds to $\phi_3 < 90^\circ$. The current experimental data is inconclusive. For example, with 29 fb^{-1} , Belle finds that

$$R = \frac{\tau^+ \mathcal{B}(B^0 \rightarrow \pi^\mp K^\pm)}{\tau^0 \mathcal{B}(B^+ \rightarrow \pi^\mp K^0)} = 1.27 \pm 0.22 \pm 0.11, \quad (20)$$

which is consistent with both possibilities.

Another important ratio of decay rates is

$$R_1 = \frac{\Gamma(B^0 \rightarrow \pi^\mp\pi^\pm)}{2\Gamma(B^\pm \rightarrow \pi^\pm\pi^0)}. \quad (21)$$

In the absence of isospin violation, this ratio should be unity. However, interference between trees and penguins, final state interactions (FSI), and the contribution of color-suppressed diagrams can reduce this ratio. Experimentally, this ratio is 0.40 ± 0.08 , far from unity.

It will be interesting to observe the pattern of these ratios with much higher statistics. For example, there is a hint in present data that rare decays favor ϕ_3 close to or greater than 90° whereas the unitarity triangle fits prefer much smaller values of ϕ_3 .¹⁸

3 Gluonic, Photonic and Electroweak Penguins

3.1 Photonic Penguins

There a large number of complications frm the strong interaction when studying $b \rightarrow sg^*$, the gluonic penguin. Instead, we now examine a simpler penguin process, the radiative penguin $b \rightarrow s\gamma$. Here the largest contribution from high mass physics, a W loop with an internal top-quark. Thus there is potential sensitivity to new physics.

The $b \rightarrow s\gamma$ decay was first observed in 1993 by CLEO in the exclusive decay channel $B \rightarrow K^*\gamma$.¹⁹ Here the s quark has hadronized into in a K^* meson. The small signal that was observed is shown in Fig. 10(a). The strongest channel $B^0 \rightarrow K^{*0}\gamma$, $K^{*0} \rightarrow K^+\pi^-$ contained 8 events over a background of 1.1 ± 0.2 events. Supporting evidence was found in the $K_S^0\pi^-$ (2 events over 0.01 background) and $K^-\pi^0$ channel (3 events over 0.8 ± 0.3 background). CLEO obtained a branching fraction of $(4.5 \pm 1.5 \pm 0.9) \times 10^{-5}$. This observation was especially significant because it was the first example of a 2nd order flavor changing neutral current in B decays.

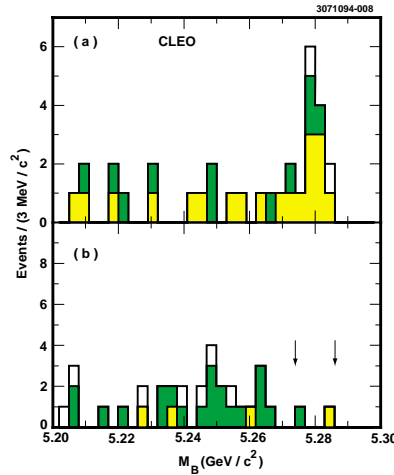


Fig. 10. The M_B projections from CLEO's first observation of a radiative penguin decay $B \rightarrow K^*\gamma$. The K^* is reconstructed in the $K^-\pi^+$, $K^-\pi^0$ and $K_S^0\pi^-$ decay modes are shown in (a).

Unfortunately there are large uncertainties associated with the hadronization of the s quark into a K^* meson, and so recent even more precise measurements by Belle and BaBar of the rate for $B \rightarrow K^*\gamma$ cannot be reliably translated into a determination of the parton level $b \rightarrow s\gamma$ rate.

However, the inclusive rate can be measured from the endpoint of the inclusive photon spectrum in B decay. The signal for $b \rightarrow s\gamma$ is expected to peak in the region $2.2 < E_\gamma < 2.7$ GeV, with only about 15% of the rate expected to lie outside this range.²⁴ The fraction outside this range is extrapolated using a theoretical calculation such as that of Neubert and Kagan. The result depends on the b quark mass, a quantity that can also be calculated from experiment.

To circumvent this problem, CLEO found techniques to measure the inclusive $b \rightarrow s\gamma$ rate.²⁰ It is quite difficult to measure an inclusive single photon signal in the midst of very large continuum backgrounds (see Fig. 11). Two experimental methods are employed to suppress the large background from non-resonant $e^+e^- \rightarrow q\bar{q}$ and initial state radiation i.e. $e^+e^- \rightarrow q\bar{q}\gamma$.

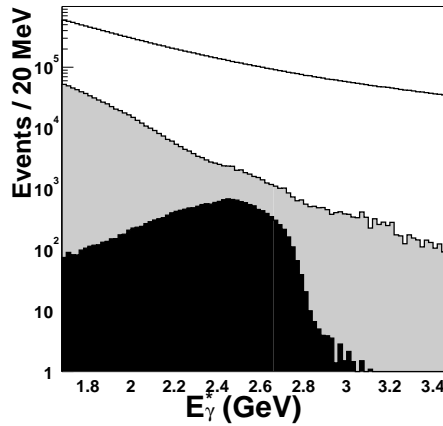


Fig. 11. A MC simulation of inclusive $b \rightarrow s\gamma$ showing the contribution of continuum and $B\bar{B}$ backgrounds. Note the vertical scale is logarithmic. The $B\bar{B}$ tail extends beyond 2.6 GeV due to the contribution of neutral hadrons.

One method uses $K(n\pi)\gamma$ combinations with $n < 4$ and at most 1 π^0 that are consistent in M_{bc} and ΔE with B candidates in order to suppress continuum. The remaining continuum background is directly subtracted and one then looks for a peak near 2.3 GeV consistent with the monochromatic photon from the quasi-two decay $b \rightarrow s\gamma$. This method of continuum suppression is called “ B reconstruction”. The resulting photon energy spectrum is shown in Fig. 12.

Examination of the observed mass of the (X_s system) particles (see fig.13) that accompany the high energy photon in $b \rightarrow s\gamma$ indicates that there are states other than $B \rightarrow K^*\gamma$ which contribute. Note that $B \rightarrow K\gamma$ is forbidden by angular momentum

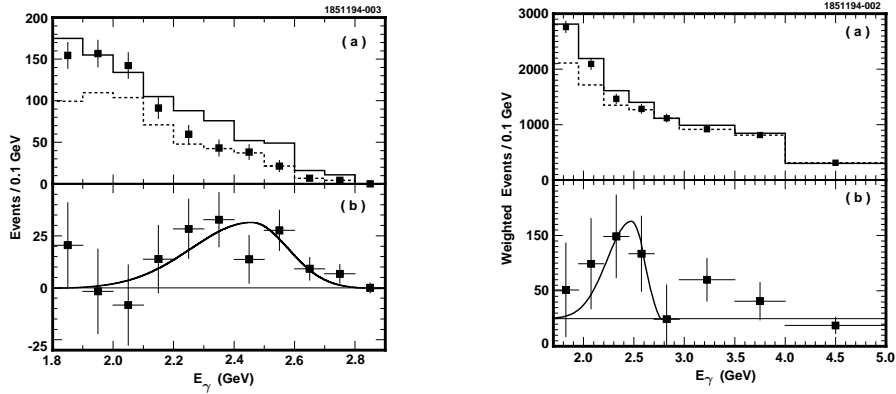


Fig. 12. The E_γ distributions from the first observation of inclusive radiative penguin decay $b \rightarrow s\gamma$ by CLEO. The distribution on the left use the B reconstruction method while those on the right use the neural network method.

conservation.

A second complementary method uses a neural net algorithm that depends on inputs from energies in cones around the photon candidate and other event shape properties to distinguish $b \rightarrow s\gamma$ signal and background. This is referred to as the neural network analysis. The network uses the event shape variables R_2 , S_\perp , R'_2 , $\cos\theta'_T$ as well as the energy deposited in cones within 20° and 30° of the photon direction and in similar cones in the direction opposite to the photon. The event shape variables with primes are calculated with the photon candidate removed and are designed to suppress initial state radiation background. The output of the neural network is a value between -1 and 1 which measures the degree to which an event resembles signal. The network is trained using a large sample of continuum Monte Carlo events. The photon energy spectrum from this method is shown in Fig. 12. Although the continuum suppression is much less effective, there is less model-dependence from hadronization uncertainty.

A third method uses lepton tagging to reduce continuum background. This is appropriate for large data samples available at the B factories and may allow the final model dependence to be reduced. An example from a recent BaBar analysis²³ is shown in Fig. 14.

The results from different methods are compared in Table 3. All the results^{20,21,22,23} are consistent and are in agreement with the NLO calculation $\mathcal{B}(b \rightarrow s\gamma) = (3.29 \pm 0.33) \times 10^{-4}$.²⁴ Note that the more inclusive methods have a smaller theoretical uncer-

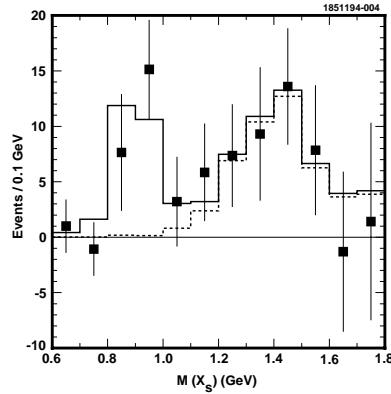


Fig. 13. The $M(X_s)$ distributions from the first observation of inclusive radiative penguin decay $b \rightarrow s\gamma$ by CLEO. This distribution uses the B reconstruction method.

Table 3. $\mathcal{B}(b \rightarrow s\gamma)$ in units of 10^{-4}

exp	technique	result
CLEO	NN+semi-inclusive	$(3.21 \pm 0.43 \pm 0.27^{+0.18}_{-0.10})$
ALEPH	NN+semi-inclusive	$(3.11 \pm 0.80 \pm 0.72)$
Belle	semi-inclusive	$(3.36 \pm 0.53 \pm 0.42 \pm 0.52)$
BaBar	semi-inclusive	$(4.3 \pm 0.5 \pm 0.8 \pm 1.3)$
BaBar	full-inclusive (lepton)	$(3.88 \pm 0.36 \pm 0.37^{+0.43}_{-0.28})$

tainty that is reflected in the size of the third error.

The branching fraction for $b \rightarrow s\gamma$ is one of the most useful constraints of extensions of the Standard Model. For example, there are over 500 citations of the original CLEO paper on inclusive $b \rightarrow s\gamma$. A well-known example of these constraints is a very restrictive lower limit on the charged Higgs mass.²⁶

Since the dominant diagrams have the same weak phase in the Standard Model, the expectation for CP violation in $b \rightarrow s\gamma$, $A_{CP}(b \rightarrow s\gamma) \sim 0.005$, is very small. This can be compared to the limit from CLEO, $-0.27 < A_{CP} < 0.10$ at 90% C.L..²⁵ More sensitive searches will also provide constraints on the extensions of the Standard Model where additional CP violating phases are possible.

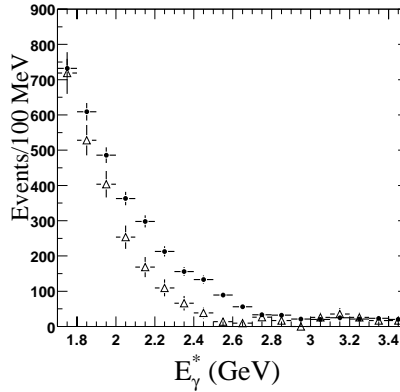


Fig. 14. The E_γ distributions from the BaBar analysis of inclusive radiative penguin decay $b \rightarrow s\gamma$. The filled points are on-resonance data, while the open points are continuum data. This analysis has a lepton tagging requirement that reduces the large continuum background.

3.2 Electroweak Penguins: $b \rightarrow s\ell^+\ell^-$

The $b \rightarrow s\gamma$ diagram can be modified by replacing the real photon by a virtual photon or by a virtual Z^0 or other neutral boson that produces a lepton pair (see Fig. 15). This penguin diagram leads to both $B \rightarrow K\ell^+\ell^-$ and $B \rightarrow K^*\ell^+\ell^-$ decays, since the $B \rightarrow K$ transition is no longer forbidden by angular momentum conservation as it was for $b \rightarrow s\gamma$. Although the penguin amplitude for $b \rightarrow s\ell^+\ell^-$ is smaller than $b \rightarrow s\gamma$ the final states can be identified easily.

As in the radiative penguin decay discussed previously, the process $b \rightarrow s\ell^+\ell^-$ is sensitive to high mass physics including charged Higgs bosons, Z' bosons and other non-standard couplings. Note, however, that the sensitivity to new physics is different from that in $b \rightarrow s\gamma$. For example, in terms of operators, $b \rightarrow s\gamma$ is sensitive to $|C_7^{eff}|$ while $b \rightarrow s\ell^+\ell^-$ one can determine the sign of C_7^{eff} as well as C_9^{eff} and C_{10} .²⁷

Using 29 fb^{-1} of data, Belle reported the first observation of the decay $B \rightarrow K\ell^+\ell^-$ ($\ell = e, \mu$) with a branching fraction of

$$\mathcal{B}(B \rightarrow K\ell^+\ell^-) = (0.75_{-0.21}^{+0.25} \pm 0.09) \times 10^{-6}$$

The first signal is shown in Fig. 16. There are 11 events over an estimated background of 1.6. The signal is larger in the dimuon channel than in the dielectron channel. However, statistics are low and both are consistent.

Initially, there was some controversy on this result since BaBar did not confirm it with a comparable dataset.³¹ Recently, BaBar has added more data and reprocessed

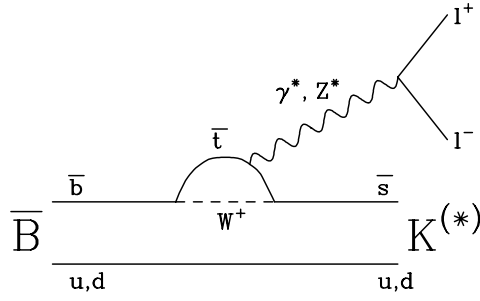


Fig. 15. Feynman diagrams for $b \rightarrow s\ell^+\ell^-$ decays. The virtual photon and Z contributions are shown.

their sample.³² They now find $\mathcal{B}(B \rightarrow K\ell^+\ell^-) = (0.78_{-0.20}^{+0.24+0.11}) \times 10^{-6}$ in agreement with the original Belle result. With more data, Belle also confirms their original result and finds²⁹ $\mathcal{B}(B \rightarrow K\ell^+\ell^-) = (0.58_{-0.15}^{+0.17} \pm 0.06) \times 10^{-6}$.

The usefulness of measurements of exclusive modes, as in the case of $b \rightarrow s\gamma$, is limited by the large theoretical uncertainties associated with the s quark to K meson hadronization process. Using an analysis procedure similar to the “ B reconstruction” technique used by CLEO to reconstruct $b \rightarrow s\gamma$, Belle observed the inclusive process $B \rightarrow X_s\ell^+\ell^-$ with 60 fb^{-1} of data. The signal is shown in Fig.18 (a),(b),(c) and contains $60.1 \pm 13.9_{-5.4}^{+8.6}$ events. The background shape is verified with the $X_s e^\pm \mu^\mp$ control sample (shown in Fig.18 (d)). The distributions of $M(X_s)$ and $M(\ell^+\ell^-)$ are shown in Fig. 19 (c),(d). Both are consistent with Monte Carlo expectations. Belle finds

$$\mathcal{B}(B \rightarrow X_s\ell^+\ell^-) = (6.1 \pm 1.4_{-1.1}^{+1.4}) \times 10^{-6}$$

with $M(\ell^+\ell^-) > 0.2 \text{ GeV}$. This can be compared to the SM expectation of $(4.15 \pm 0.7) \times 10^{-6}$.²⁷ Note that the dilepton mass requirement eliminates the pole from $b \rightarrow s\gamma^*, \gamma^* \rightarrow e^+e^-$. Hence the expected branching fractions in the dimuon and dielectron channels should be approximately equal.

In addition to the rate, there are other important observables that are sensitive to physics beyond the Standard Model. One example is the $M(\ell^+\ell^-)$ distribution. This distribution is shown in Fig.17 for the original sample of exclusive $B \rightarrow K\ell^+\ell^-$ candidates and compared to the Standard Model Monte Carlo. The corresponding distribution is shown in Fig. 19(c) for the inclusive $X_s\ell^+\ell^-$ sample. New physics can modify this distribution at either low mass or high mass. However, care must be taken to un-

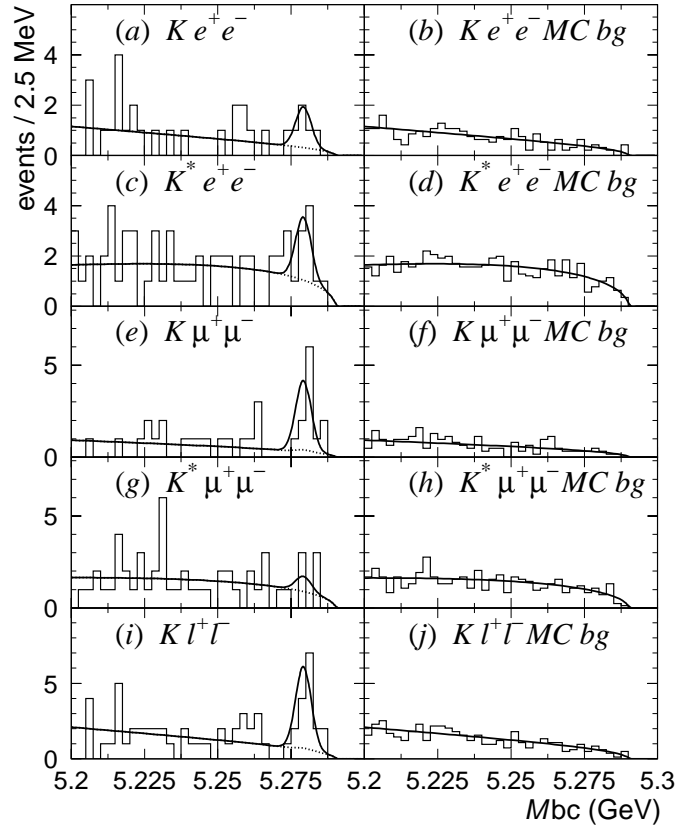


Fig. 16. The left column shows Belle data while the right column are MC simulations of background. The Belle distributions of M_{bc} for: (a),(b) Ke^+e^- candidates and MC background (c),(d) $K^*e^+e^-$ candidates and MC background (e), (f) $K\mu^+\mu^-$ candidates and MC background, (g), (h) $K^*\mu^+\mu^-$ candidates and MC background, (i), (j) combined $K\ell^+\ell^-$ candidates and MC background.

derstand the contribution of SM long distance effects.²⁷ At the moment, however, the statistics are too low to draw any strong conclusions.

4 Mysteries and Open Questions

In the future, there are several aspects of rare decays that may be especially interesting in the future. These include the search for direct CPV, more detailed examination of $b \rightarrow s\ell^+\ell^-$ decays, $B \rightarrow \eta'X_s$ decays and the study of CPV in $b \rightarrow s$ penguin modes such as $B \rightarrow \phi K_S^0$. I comment briefly on each of these topics below.

Where is the direct CP violation in B decay? Although the expected asymmetries in rare B decays are orders of magnitude larger than those in kaon decay such as ϵ'/ϵ

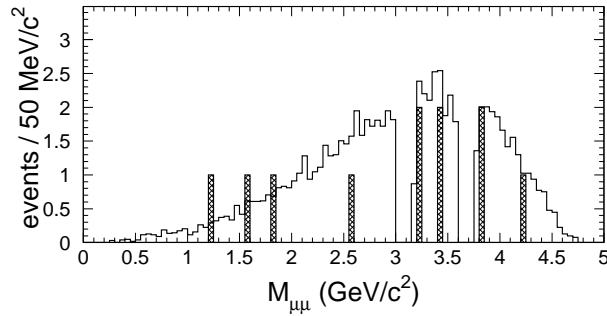


Fig. 17. The Belle distributions of $M(\ell^+\ell^-)$ for the $K\ell^+\ell^-$ candidates. The distribution is compared to the expectation from a Monte Carlo simulation based on the Standard Model.

(discussed in the SSI lectures by Tschirhart), very large data samples are needed to observe them. So far, there are only upper limits in hadronic B decay modes (see Table 2) except for the case of $B \rightarrow \pi^+\pi^-$, where the experimental situation is still unsettled. Currently, BaBar finds $A_{\pi\pi} = 0.30 \pm 0.25 \pm 0.04$ ⁴⁵ while Belle finds a hint of an asymmetry ($\sim 2.9\sigma$ level) $A_{\pi\pi} = 0.77 \pm 0.27 \pm 0.08$.⁴⁶ In addition to searches in modes with contributions from both tree and penguin diagrams, it will also be important to look for direct CPV in pure penguin processes such as $B^\pm \rightarrow K_S^0\pi^\pm$ and $b \rightarrow s\gamma$ where new physics sources of CPV might appear.

As discussed above, the exclusive decay $B \rightarrow K\ell^+\ell^-$ and inclusive process $b \rightarrow s\ell^+\ell^-$ have now been experimentally established. Examination of the $M(\ell^+\ell^-)$ spectrum will be important. With more data it should also be possible to finally observe $B \rightarrow K^*\ell^+\ell^-$. High statistics of this decay mode are especially interesting. One observable, the forward-backward asymmetry (A_{FB}), with respect to the polar angle of the lepton in the dilepton rest-frame is a particularly good diagnostic for new physics. The dependence of A_{FB} on q^2 , the invariant mass of the dilepton system, can be dramatically altered in new physics scenarios such as SUSY or SUGRA.²⁷ This type of study will, however, require the enormous data samples of a super B-factory.

CLEO first observed the decay $B^+ \rightarrow \eta'K^+$.³³ This decay mode is the largest rare B decay with a branching fraction of $(80_{-9}^{+10} \pm 7) \times 10^{-5}$ (CLEO), more than three times the rate of $B^0 \rightarrow K^-\pi^+$. However, $B^+ \rightarrow \eta'\pi^+$ is not observed. CLEO also found sizeable branching fractions for the decays $B \rightarrow \eta K^{*0}$ as well. However, the corresponding η' decay mode, $B \rightarrow \eta'K^*$ has not been observed. The experimental results are summarized in Table 4. BaBar³⁶ and Belle³⁵ have confirmed the CLEO

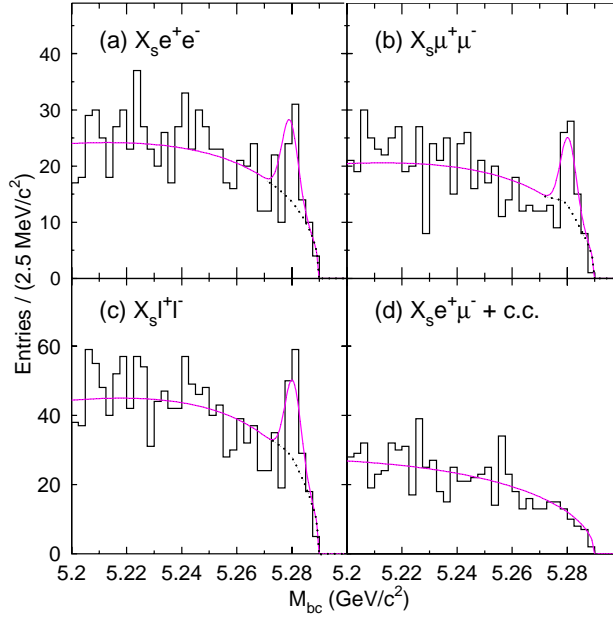


Fig. 18. The Belle distributions of M_{bc} for: (a) $X_s \mu^+ \mu^-$ candidates, (b) $X_s e^+ e^-$, (c) $X_s \ell^+ \ell^-$ candidates and the (d) $X_s e^\pm \mu^\mp$ control sample.

results with more precision.

Lipkin has proposed a plausible explanation of the enhanced rates for $B \rightarrow \eta' K$ and $B \rightarrow \eta K^*$ in terms of constructive interference of the diagrams involving the $u\bar{u}$ and $s\bar{s}$ components of the η' and η wavefunctions,³⁸ shown in Figs. 20(a),(b).

In addition to these large exclusive decay modes, CLEO reported the observation of inclusive $B \rightarrow \eta' X_s$ at a high rate,

$$\mathcal{B}(B \rightarrow \eta' X_s) = (6.2 \pm 1.6 \pm 1.3_{-1.5}^{+0.0}) \times 10^{-4}.$$

The first and second errors are statistical and systematic, respectively. The third asymmetric error is due to the possibility of background from color-suppressed $b \rightarrow c$ decays such as $\bar{B}^0 \rightarrow D^0 \eta'$. Approximately 10% of the inclusive yield comes from the exclusive decay mode $B^- \rightarrow \eta' K^-$. There is no significant excess in the K^* mass region. The remainder of the yield comes from events with X_s mass near or above charm threshold (1.8 GeV). This result has recently been confirmed by preliminary BaBar results.³⁷

A number of interpretations have been proposed to account for this experimental result. These include: (I) conventional $b \rightarrow sq\bar{q}$ operators with constructive interference between the $u\bar{u}$, $d\bar{d}$, and $s\bar{s}$ components of the η' ,³⁸ (II) $b \rightarrow c\bar{c}s$ decays enhanced by $c\bar{c}$ content in the η' wavefunction,^{39,40} and (III) $b \rightarrow sg^*, g^* \rightarrow g\eta'$ from the η' QCD

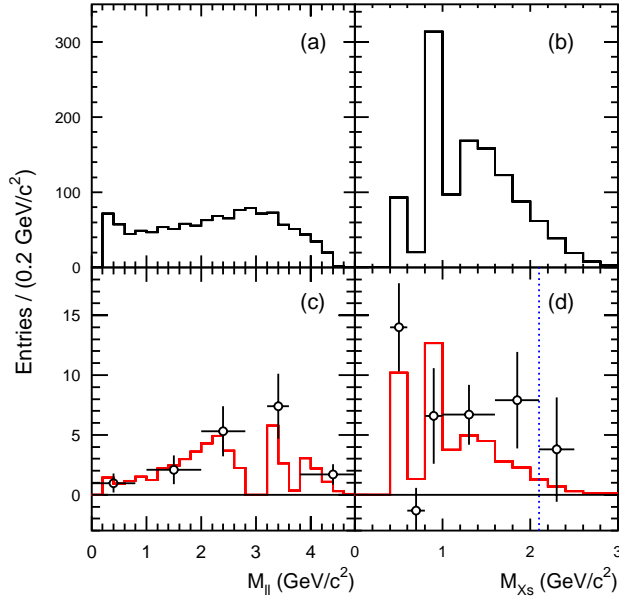
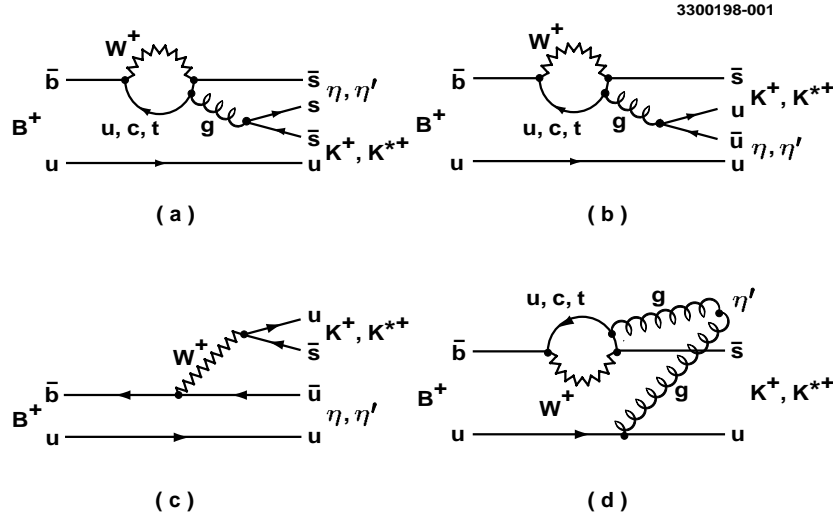


Fig. 19. The generated Monte Carlo distributions of (a) X_s mass, (b) $M(\ell^+ \ell^-)$ for $B \rightarrow X_s \ell^+ \ell^-$ decays. The Belle background subtracted distributions for: (c) X_s mass and (d) $M(\ell^+ \ell^-)$ compared to the reconstructed Monte Carlo distributions. The analysis includes a cut $M(X_s) < 2.1$ GeV, indicated by the dotted vertical line.

anomaly, which also accounts for the large mass of the η' relative to other members of its SU(3) multiplet.^{41,42} Each of these theoretical scenarios should lead to a characteristic X_s mass spectrum and other distinctive features. For example, the first two scenarios will give a X_s mass distribution peaked near 1.5 GeV while the third scenario gives a three body $gs\bar{q} X_s$ mass spectrum which peaks above 2 GeV. The third scenario appears to be most consistent with the distribution observed in the $M(X_s)$ spectrum of data.

Although this third scenario appears to offer the most promising explanation, Kagan and Petrov pointed out that the slowly decreasing $\eta' g^* g$ form factor required for this explanation would have other experimental consequences in $\Upsilon(1S) \rightarrow \eta' X$ decays.⁴³ The rate for such $\Upsilon(1S) \rightarrow \eta'$ decays has recently been measured by CLEO.⁴⁴ The observed η' momentum spectrum does not support the large and slowly decreasing form factor.⁴⁴ Hence the inclusive $B \rightarrow \eta' X$ decays remain problematic and might even require new physics.

In addition to the program of measuring the angles of the unitarity triangle (discussed in the SSI lectures by MacFarlane), there is also the question of whether there are new CP violating phases from new interactions or physics beyond the Standard


 Fig. 20. Feynman diagrams that contribute to rare B decays with η' mesons.

Model. At the moment, such new phases are very poorly constrained. One way to attack this question is to measure the time dependent CP asymmetry in $b \rightarrow s$ penguin modes such as $B^0 \rightarrow \phi K_S^0$ or $B^0 \rightarrow \eta' K_S^0$ and compare it to the asymmetry in $B^0 \rightarrow \psi K_S^0$. In the absence of new physics, they should be equal. However, if there are new physics contributions in penguin loops these asymmetries will differ substantially. For $B^0 \rightarrow \eta' K_S^0$, Belle finds $\sin(2\phi)^{eff} = 0.71 \pm 0.37_{-0.06}^{+0.05}$, in good agreement with the charmonium modes.⁴⁷ With current data, an intriguing discrepancy has developed in the $b \rightarrow s\bar{s}s$ penguin dominated mode, $B^0 \rightarrow \phi K_S^0$. Here

 Table 4. Branching Fractions in units of 10^{-6} for $B \rightarrow K(\pi)\eta'$ and $B \rightarrow K^*\eta(\eta')$ Modes.

	BaBar	Belle	CLEO
$B^- \rightarrow \eta' K^-$	$70 \pm 8 \pm 5$	$77.9_{-5.9}^{+6.2} \pm 9.0$	$80_{-9}^{+10} \pm 7$
$B^0 \rightarrow \eta' K^0$	$42_{-11}^{+13} \pm 4$	$68.0_{-9.6}^{+10.4} \pm 8.0$	$89_{-16}^{+18} \pm 9$
$B^- \rightarrow \eta' \pi^-$	$5.4_{-2.6}^{+3.5} \pm 0.87$		< 12
$B^- \rightarrow \eta K^{*-}$	$22.1_{-9.2}^{+11.1} \pm 3.3$	$26.5_{-7.0}^{+7.8} \pm 3.0$	$26.4_{-8.2}^{+9.6} \pm 3.3$
$B^0 \rightarrow \eta K^{*0}$	$19.8_{-5.6}^{+6.5} \pm 1.7$	$16.5_{-4.2}^{+4.6} \pm 1.2$	$13.8_{-4.6}^{+5.5} \pm 1.6$
$B^- \rightarrow \eta K^-$			< 6.9

Belle finds $\sin(2\phi)^{eff} = -0.73 \pm 0.64 \pm 0.22$ while BaBar obtains $\sin(2\phi)^{eff} = -0.19_{-0.50}^{+0.52} \pm 0.09$.^{48,47} The weighted average, $-0.29_{-0.41}^{+0.42}$, is 2.7σ from the Standard Model expectation of 0.73 ± 0.055 , the value in charmonium modes. Again an order of magnitude more data is needed for stringent tests. This search for new physics in CPV has already stimulated a great deal of theoretical interest⁴⁹ and will be one of the most interesting aspects of the next phase in B factory physics.

References

- [1] P. Darrriulat et al., Phys. Lett. **B 33**, 249 (1970).
- [2] S. L. Glashow, J. Iliopoulos, and L. Maiani, Phys. Rev. **D 2** 1285 (1970).
- [3] M. K. Gaillard, B. W. Lee and J. L. Rosner, Rev. Mod. Phys. **47** 277 (1975).
- [4] J. J. Aubert et al., Phys. Rev. Lett. **33** 1404 (1974). J. E. Augustin et al., Phys. Rev. Lett. **33** 1406 (1974).
- [5] A. Chen et al., Phys Lett. **B 122**, 317 (1983).
- [6] H. Albrecht et al., Phys. Lett. **B 192**, 245 (1987).
- [7] V.D. Barger, T. Han, D.V. Nanopoulos and R.J.N. Phillips, Phys. Lett. **B 194**, 312 (1987).
- [8] G. Arnison et al. (UA1 Collaboration), Phys. Lett. **B 122**, 103 (1983); R. M. Godbole, S. Pakvasa and D.P. Roy, Phys. Rev. Lett. **50**, 1539 (1983).
- [9] M. A. Shifman, *ITEP Lectures on Particle Physics and Field Theory*, 1st ed. (World Scientific, Singapore, 1999).
- [10] G. C. Fox and S. Wolfram, Phys. Rev. Lett. **41**, 1581 (1978).
- [11] H. Albrecht et al. (ARGUS Collaboration), Phys. Lett. **B 192**, 245 (1987).
- [12] M. Neubert, hep-ph/0207357, Proceedings of the 37th Rencontres de Moriond.
- [13] B. C. K. Casey et al. (Belle Collaboration), Phys. Rev. **D 66** 092002 (2002). The limit on asymmetry in $B^\pm \rightarrow K_S^0 \pi^\pm$ was updated with more data. See the contribution of B.C.K. Casey to the Proceedings of the Topical Conference.
- [14] B. Aubert et al. (BaBar Collaboration), Phys. Rev. Lett. **89**, 281802 (2002); B. Aubert et al. (BaBar Collaboration), hep-ex/0207065.
- [15] D. Cronin-Hennessy *et al.* (CLEO Collaboration), Phys. Rev. Lett. **85**, 515 (2000); S. Chen *et al.* (CLEO Collaboration), Phys. Rev. Lett. **85**, 525 (2000).

- [16] R. Fleischer and T. Mannel, hep-ph/9704423, Phys. Rev. **D 57**, 2752 (1998).
- [17] Z. Ligeti, hep-ph/0302031, to appear in the Proceedings of the SLAC 2002 summer institute.
- [18] For recent discussions, see M. Neubert, hep-ph/021794 and C-K. Chua, W-S. Hou and K-C. Yang, hep-ph/021002.
- [19] R. Ammar et al. (CLEO Collaboration), Phys. Rev. Lett. **71**, 674 (1993).
- [20] M. S. Alam et al. (CLEO Collaboration), Phys. Rev. Lett. **74**, 2885 (1995); S. Chen et al. (CLEO Collaboration), Phys. Rev. Lett. **87**, 251807 (2001).
- [21] R. S. Barate et al. (ALEPH Collaboration), Phys. Lett. **B 511**, 151 (2001).
- [22] K. Abe et al. (Belle Collaboration), Phys. Lett. **B 511**, 151 (2001).
- [23] B. Aubert et al. (BaBar Collaboration), hep-ex/0207076; B. Aubert et al. (BaBar Collaboration), hep-ex/0207074.
- [24] M. Neubert and A. Kagan, Eur. Phys. J C **7**, 5 (1999).
- [25] T.E. Coan et al. (CLEO Collaboration), Phys. Rev. Lett. **86**, 5661 (2001).
- [26] Some examples and additional references are given in J. L. Hewett and J. D. Wells, Phys. Rev. **D 55**, 5549 (1997); J. L. Hewett, hep-ph/940632.
- [27] A. Ali, C. Greub and G. Hiller, Phys. Rev. **D 66**, 034002 (2002).
- [28] K. Abe et al. (Belle Collaboration), Phys. Rev. Lett. **90**, 021801 (2003).
- [29] K. Abe et al. (Belle Collaboration), BELLE-CONF-0241, paper contributed to the ICHEP2002 conference.
- [30] J. Kaneko et al. (Belle Collaboration), Phys. Rev. Lett. **88**, 021801 (2002).
- [31] B. Aubert et al. (BaBar Collaboration), Phys. Rev. Lett. **88**, 241801 (2002).
- [32] B. Aubert et al. (BaBar Collaboration), hep-ex/0207082, paper contributed to the ICHEP2002 conference.
- [33] B. Behrens et al. (CLEO Collaboration), Phys. Rev. Lett. **80**, 3710 (1998).
- [34] T. E. Browder et al. (CLEO Collaboration), Phys. Rev. Lett. **81**, 1786 (1998).
- [35] K. Abe et al., Phys. Lett. **B 517**, 309 (2001).
- [36] B. Aubert et al., Phys. Rev. Lett. **87**, 221802 (2001).
- [37] B. Aubert et al. (BaBar Collaboration), hep-ex/0109034.

- [38] H.J. Lipkin, Phys. Lett. B. 254, 247 (1991).
- [39] I. Halperin and A. Zhitnitsky, hep-ph/9704412 Phys. Rev. D. **56**, 7247 (1997); I. Halperin and A. Zhitnitsky, hep-ph/9705251, Phys. Rev. Lett **80** 438 (1998); E. Shuryak and A. Zhitnitsky, hep-ph/9706316, Phys. Rev. D **57**, 2001 (1998).
- [40] F. Yuan and K-T. Chao, hep-ph/9706294. Phys. Rev. D **56**, 2495 (1997).
- [41] D. Atwood and A. Soni, hep-ph/9704357. Phys. Lett. B **405** 150, (1997).
- [42] W-S. Hou and B. Tseng, hep-ph/9705304, Phys. Rev. Lett **80**, 434 (1998).
- [43] A.L. Kagan and A.A. Petrov, hep-ph/9707354.
- [44] M. Artuso et al. (CLEO Collaboration), CLNS 02/1805, submitted to Phys. Rev. D.
- [45] B. Aubert et al., hep-ex/0207055, to be published in Phys. Rev. Lett.
- [46] K. Abe et al., hep-ex/0301032, submitted to Phys. Rev. D.
- [47] K. Abe et al., hep-ex/0212062, to appear in Phys. Rev. D.
- [48] B. Aubert et al., BABAR-CONF-02/016, SLAC-PUB-9297, hep-ex/0207070.
- [49] A. Kundu and T. Mitra, hep-ph/0302123; C-W Chiang and J. Rosner, hep-ph/0302094; S. Baek, hep-ph/0301269; S. Khalil and E. Kou, hep-ph/0212023; G.L. Kane, P. Ko, C. Kolda, Jae-Hyeon Park, Haibin Wang, Lian-Tao Wang, hep-ph/0212092; J-P Lee, K. Y. Lee, hep-ph/0209290; B. Dutta, C.S. Kim and S. Oh, hep-ph/0208226, Phys. Rev. Lett. **90**, 011801 (2002); M. Raidal, hep-ph/0208091, Phys. Rev. Lett. **89**, 231803 (2002); M. Ciuchini, L. Silvestrini, hep-ph/0208087, PRL 89, 231802 (2002); A. Datta, hep-ph/0208016, Phys. Rev. D **66**, 071702 (2002); H. Murayama, hep-ph/0208005; G. Hiller, hep-ph/0207356, Phys. Rev. D **66**, 071502 (2002); M-B. Causse, hep-ph/0207070; Y. Nir, hep-ph/0208080; Y. Grossman, G. Isidori and M. P. Worah, Phys. Rev. D **58**, 057504 (1998); R. Fleischer and T. Mannel, hep-ph/0103121. D. London and A. Soni, Phys. Lett B **407**, 61 (1997); Y. Grossman and M. P. Worah, Phys Lett. B **395**, 241 (1997);